JOC Featured Article

pubs.acs.org/joc

Concerning the Hydrolytic Stability of 8-Aryl-2′-deoxyguanosine Nucleoside Adducts: Implications for Abasic Site Formation at Physiological pH

Katherine M. Schlitt,[†] Ke-wen M. Sun,[†] Robert J. Paugh,[†] Andrea L. Millen,[‡] Lex Navarro-Whyte,[‡] Stacey D. Wetmore,*[,‡] and Richard A. Manderville*[,†]

[†]*Department of Chemistry, University of Guelph, Guelph, Ontario, Canada N1G 2W1, and* [‡]*Department of Chemistry, University of Lethbridge, Lethbridge, Alberta, Canada T1K 3M4*

rmanderv@uoguelph.ca; stacey.wetmore@uleth.ca

Received May 22, 2009

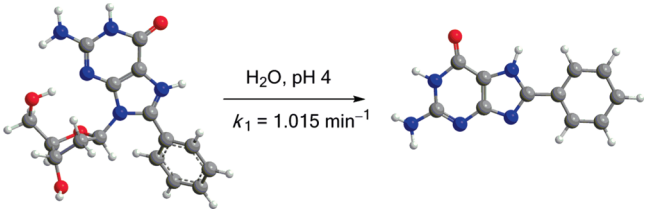

Direct addition of aryl radical species to the C^8-site of 2′-deoxyguanosine (dG) affords C^8-aryl-dG adducts that are produced by carcinogenic arylhydrazines, polycyclic aromatic hydrocarbons (PAHs), and certain phenolic toxins. A common property of C^8-arylpurine adduction is the accompaniment of abasic site formation. To determine how the C^8-aryl moiety contributes to sugar loss, UV−vis spectroscopy has been employed to determine N^7 pK_{a1} values and hydrolysis kinetics, while density functional theory (DFT) calculations have been utilized to probe the structural features and stability of the C^8-aryl-dG adducts bearing different para and ortho substituents. In all cases, the C^8-aryl-dG adducts adopt a *syn* conformation containing a strong $O^{5'}-H\cdots N^3$ hydrogen bond with the aryl ring twisted with respect to the nucleobase. The adducts undergo N^7-protonation with ionization constants and calculated N^7 proton affinity (PA) values similar to those measured for dG. The hydrolysis kinetics shows that C^8-aryl-dG nucleoside adducts are more prone than dG to acid-catalyzed hydrolysis, with those bearing para substituents having k_1 values that are ca. 90- to 200-fold larger than k_1 for dG, while the effects for the ortho adducts are only ca. 9- to 60-fold larger. Changes in the rate of hydrolysis are further explained by calculations showing that glycosidic bond cleavage in the *syn* orientation of both neutral and N^7-protonated dG has a lower barrier than the *anti* orientation, and the bulky (phenyl) group further decreases the barrier. Despite adduct reactivity in acidic media, all adducts are relatively stable at physiological pH with $t_{1/2}$ ~25 days, suggesting that they are unlikely intermediates leading to abasic site formation at physiological pH. This information has allowed development of a new rationale for the tendency of abasic site formation to accompany C^8-arylpurine adduction within duplex DNA at neutral pH.

Introduction

DNA modification is an early event in the carcinogenic process,[1] and modified nucleosides serve as biomarkers for exposure to chemical carcinogens that form covalent DNA adducts.[2,3] Modified nucleobases are also used as bioprobes,[4] therapeutics,[5] or designer molecules such as fleximers.[6] Our

(1) Josephy, P. D.; Mannervik, B. *Molecular Toxicology*, 2nd ed.; Oxford University Press, Inc.: New York, 2006; pp 46−82.
(2) Hoffmann, G. R.; Fuchs, R. P. P. *Chem. Res. Toxicol.* **1997**, *10*, 347–359.
(3) Stover, J. S.; Ciobanu, M.; Cliffel, D. E.; Rizzo, C. J. *J. Am. Chem. Soc.* **2007**, *129*, 2074–2081.
(4) (a) Kool, E. T. *Acc. Chem. Res.* **2002**, *35*, 936–943. (b) Lynch, S. R.; Liu, H. B.; Gao, J. M.; Kool, E. T. *J. Am. Chem. Soc.* **2006**, *128*, 14704–14711. (c) Ogawa, A. K.; Abou-Zied, O. K.; Tsui, V.; Jimenez, R.; Case, D. A.; Romesberg, F. E. *J. Am. Chem. Soc.* **2000**, *122*, 9917–9920.
(5) (a) Galmarini, C. M.; Mackey, J. R.; Dumontet, C. *Lancet Oncol.* **2002**, *3*, 415–424. (b) Sigmond, J.; Peters, G. J. *Nucleosides Nucleotides Nucleic Acids* **2005**, *24*, 1997–2022.
(6) (a) Polak, M.; Seley, K. L.; Plavec, J. *J. Am. Chem. Soc.* **2004**, *126*, 8156–8166. (b) Bardon, A. B.; Wetmore, S. D. *J. Phys. Chem. A* **2005**, *109*, 262–272.

DOI: 10.1021/jo901080w Published on Web 07/16/2009

interest in modified nucleosides stems from research on DNA adduction by phenolic toxins that undergo metabolic activation to form phenoxyl radical intermediates that can attach covalently to the C^8-site of 2′-deoxyguanosine (dG).[7] Due to the ambident (*O*- vs *C*-attack) reactivity of phenoxyl radicals both *O*- and *C*-linked adducts are produced, as exemplified by *O*-PCP-8-dG (Figure 1) derived from pentachlorophenol (PCP)[8] and *C*-OTA-8-dG derived from the mycotoxin ochratoxin A (OTA).[9] Other phenolic *C*-adducts shown in Figure 1 that are likely formed from phenoxyl radical intermediates include those derived from nickel(II)−salen complexes, such as the metallopeptide−PNA bioconjugate (*C*-Ni(II)salen-8-dG)[10] that have been isolated and characterized by the Burrows laboratory. The hydroquinone adduct *C*-(3,4-EQ)-8-dG is formed from reductive activation of 3,4-estrone quinone (3,4-EQ) that yields semiquinone radical intermediates.[11] These phenolic *C*-adducts are structurally related to a family of C^8-aryl adducts. Examples include 6-BP-8-dG that is formed from the polycyclic aromatic hydrocarbon (PAH) benzo[*a*]pyrene (BP)[12] and *N*-Ac-ABA-8-dG that is derived from the powerful PAH mutagen 3-nitrobenzanthrone (NBA).[13] Oxidation of PAHs by CYP peroxidase to yield PAH radical cations facilitates C^8-aryl adduct formation.[14] Carcinogenic arylhydrazines that produce aryl radical intermediates also form C^8-aryl adducts that contain phenyl (Ph) groups bearing various para (*p*) substituents (i.e., X-Ph-8-dG, X = COOH, CH_2OCH_3, CH_2OH, Figure 1).[15]

A common property of C^8-aryl adduction is the accompaniment of abasic site formation in studies carried out at physiological pH. Treatment of DNA with BP in aqueous media with horseradish peroxidase (HRP)/HOOH afforded 6-BP-8-dG from the enzymatic digest of the precipitated DNA, while the supernatant contained roughly the same concentration of the corresponding 6-BP-8-G adduct.[12a] Significant levels of abasic site formation has also been reported for arylhydrazine treatment of DNA.[15e] Akanni and Abul-Hajj proposed that *C*-(3,4-EQ)-8-dG (Figure 1) is formed as an intermediate prior to the loss of the deoxyribose sugar to afford *C*-(3,4-EQ)-8-G.[11c] Overall, these results have led to proposals that formation of abasic sites following C^8-aryl adduct formation may contribute to the carcinogenicity of PAHs[14] and arylhydrazines.[15e]

For unmodified dG it is well-known that development of a positive charge at N^7, either through protonation[16] (pK_a for protonated dG is 2.34[17]) or alkylation,[18] accelerates the rate of hydrolysis. Acid-catalyzed hydrolysis of dG proceeds via an A-1 mechanism involving equilibrium protonation (at N^7 for the monocation and N^3 for the dication), which precedes the unimolecular rate-limiting cleavage of the C−N bond.[16] Substitution of dG with electron-withdrawing NO_2[19] and SO_2CH_3[20] C^8-substituents greatly accelerates hydrolysis, while electron-donating NH_2[21] and OCH_3[22] C^8-substituents decreases the rate of hydrolysis. Interestingly, bulky electron-donating arylamino[23] and dimethylamino[21] C^8-substituents accelerate hydrolysis compared to the unmodified base despite their electron-donating character. This has been ascribed to release of steric strain upon removal of the deoxyribose moiety.[23,24]

Because the loss of sugar from C^8-aryl adducts at neutral pH was unexpected,[12,15] we sought to determine rates of hydrolysis for the C^8-Ph-dG adducts **1**−**3c** (Figure 1) that bear para (*p*)-(**2a**−**2e**) and ortho (*o*)-substituents (**3a**−**3c**) of varying electronic and steric properties. These adducts are readily prepared using palladium-catalyzed Suzuki cross-coupling reactions[25] and include the known arylhydrazine-derived phenyl adduct **1**,[15] the isomeric *C*-phenolic adducts **2a** and **3a** formed from reactions of DNA with mutagenic diazoquinones,[26] and others serving as structural models for C^8-aryl adducts in general. To determine how the C^8-aryl moiety contributes to sugar loss for adducts **1**−**3c**, we have measured rates of hydrolysis in aqueous solutions of varying acidity and employed density functional theory (DFT) calculations to assist interpretation of the kinetic experiments. Our observations have led to the development of a new rationale for the noted tendency of abasic site formation to

(7) (a) McLaughlin, C. K.; Lantero, D. R.; Manderville, R. A. *J. Phys. Chem. A*. **2006**, *110*, 6224–6230. (b) Sun, K. M.; McLaughlin, C. K.; Lantero, D. R.; Manderville, R. A. *J. Am. Chem. Soc*. **2007**, *129*, 1894–1895. (c) Weishar, J. L.; McLaughlin, C. K.; Baker, M.; Gabryelski, W.; Manderville, R. A. *Org. Lett*. **2008**, *10*, 1839–1842.

(8) (a) Dai, J.; Wright, M. W.; Manderville, R. A. *Chem. Res. Toxicol*. **2003**, *16*, 817–821. (b) Dai, J.; Sloat, A. L.; Wright, M. W.; Manderville, R. A. *Chem. Res. Toxicol*. **2005**, *18*, 771–779.

(9) (a) Dai, J.; Wright, M. W.; Manderville, R. A. *J. Am. Chem. Soc*. **2003**, *125*, 3716–3717. (b) Dai, J.; Park, G.; Perry, J. L.; Il'ichev, Y. V.; Bow, D. A. J.; Pritchard, J. B.; Pfohl-Leszkowicz, A.; Manderville, R. A.; Simon, J. D. *Acc. Chem. Res*. **2004**, *37*, 874–881. (c) Faucet, V.; Pfohl-Leszkowicz, A.; Dai, J.; Castegnaro, M.; Manderville, R. A. *Chem. Res. Toxicol*. **2004**, *17*, 1289–1296.

(10) (a) Stemmler, A. J.; Burrows, C. J. *J. Am. Chem. Soc*. **1999**, *121*, 6956–6957. (b) Kornyushyna, O.; Stemmler, A. J.; Graybosch, D. M.; Bergenthal, I.; Burrows, C, J. *Bioconjugate Chem*. **2005**, *16*, 178–183.

(11) (a) Abul-Hajj, Y. J.; Tabakovic, K.; Tabakovic, I. *J. Am. Chem. Soc*. **1995**, *117*, 6144–6145. (b) Akanni, A.; Abul-Hajj, Y. J. *Chem. Res. Toxicol*. **1997**, *10*, 760–766. (c) Akanni, A.; Abul-Hajj, Y. J. *Chem. Res. Toxicol*. **1999**, *12*, 1247–1253.

(12) (a) Rogan, E. G.; Cavalieri, E. L.; Tibbels, S. R.; Cremonesi, P.; Warner, C. D.; Nagel, D. L.; Tomer, K. B.; Cerny, R. L.; Gross, M. L. *J. Am. Chem. Soc*. **1988**, *110*, 4023–4029. (b) Cavalieri, E. L.; Rogan, E. G.; Li, K.-M.; Todorovic, R.; Ariese, F.; Jankowiak, R.; Grubor, N.; Small, G. J. *Chem. Res. Toxicol*. **2005**, *18*, 976–983.

(13) Enya, T.; Kawanishi, M.; Suzuki, H.; Matsui, S.; Hisamatsu, Y. *Chem. Res. Toxicol*. **1998**, *11*, 1460–1467.

(14) (a) Cavalieri, E.; Rogan, E. *Environ. Health Persp*. **1985**, *64*, 69–84. (b) Cavalieri, E. L.; Rogan, E. G. *Pharmac. Ther*. **1992**, *55*, 183–199. (c) Chakravarti, D.; Pelling, J. C.; Cavalieri, E. L.; Rogan, E. G. *Proc. Natl. Acad. Sci. U.S.A*. **1995**, *92*, 10422–10426.

(15) (a) Lawson, T.; Gannett, P. M.; Yau, W.-M.; Dalal, N. S.; Toth, B. *J. Agric. Food Chem*. **1995**, *43*, 2627–2635. (b) Hiramoto, K.; Kaku, M.; Sueyoshi, A.; Fujise, M.; Kikugawa, K. *Chem. Res. Toxicol*. **1995**, *8*, 356–362. (c) Gannett, P. M.; Lawson, T.; Miller, M.; Thakkar, D. D.; Lord, J. W.; Yau, W.-M.; Toth, B. *Chem.-Biol. Interact* **1996**, *101*, 1–25. (d) Kohda, K.; Tsunomoto, H.; Kasamatsu, T.; Sawamura, F.; Terashima, I.; Shibutani, S. *Chem. Res. Toxicol*. **1997**, *10*, 1351–1358. (e) Gannett, P. M.; Powell, J. H.; Rao, R.; Shi, X.; Lawson, T.; Kolar, C.; Toth, B. *Chem. Res. Toxicol*. **1999**, *12*, 297–304.

(16) (a) Zoltewicz, D.; Clark, D. F.; Sharpless, T. W.; Grahe, G. *J. Am. Chem. Soc*. **1970**, *92*, 1741–1750. (b) Hevesi, L.; Wolfson-Davidson, E.; Nagy, J. B.; Nagy, O. B.; Bruylants, A. *J. Am. Chem. Soc*. **1972**, *94*, 4715–4720. (c) Zoltewicz, J. A.; Clark, D. F. *J. Org. Chem*. **1972**, *37*, 1193–1197.

(17) Da Costa, C. P.; Sigel, H. *Inorg. Chem*. **2003**, *42*, 3475–3482.

(18) Gates, K. S.; Nooner, T.; Dutta, S. *Chem. Res. Toxicol*. **2004**, *17*, 839–856.

(19) (a) Yermilov, V.; Rubio, J.; Ohshima, H. *FEBS Lett*. **1995**, *376*, 207–210. (b) Tretyakova, N. Y.; Burney, S.; Pamir, B.; Wishnok, J. S.; Dedon, P. C.; Wogan, G. N.; Tannenbaum, S. R. *Mutat. Res*. **2000**, *447*, 287–303.

(20) Laayoun, A.; Décout, J.-L.; Lhomme, J. *Tetrahedron Lett*. **1994**, *35*, 4989–4990.

(21) Jordan, F.; Niv, H. *Nucleic Acids Res*. **1982**, *10*, 4339–4349.

(22) Garrett, E. R.; Mehta, P. J. *J. Am. Chem. Soc*. **1972**, *94*, 8532–8541.

(23) Novak, M.; Ruenz, M.; Kazerani, S.; Toth, K.; Nguyen, T.-M.; Heinrich, B. *J. Org. Chem*. **2002**, *67*, 2303–2308.

(24) Hovinen, J.; Glemarec, C.; Sandström, A.; Sund, C.; Chattopadhyaya, J. *Tetrahedron* **1991**, *47*, 4693–4708.

(25) (a) Western, E. C.; Daft, J. R.; Johnson, E. M. II; Gannett, P. M.; Shaughnessy, K. H. *J. Org. Chem*. **2003**, *68*, 6767–6774. (b) Western, E. C.; Shaughnessy, K. H. *J. Org. Chem*. **2005**, *70*, 6378–6388. (c) Dai, Q.; Xu, D.; Lim, K.; Harvey, R. G. *J. Org. Chem*. **2007**, *72*, 4856–4863.

(26) Kikugawa, K.; Kato, T.; Kojima, K. *Mutat. Res*. **1992**, *268*, 65–75.

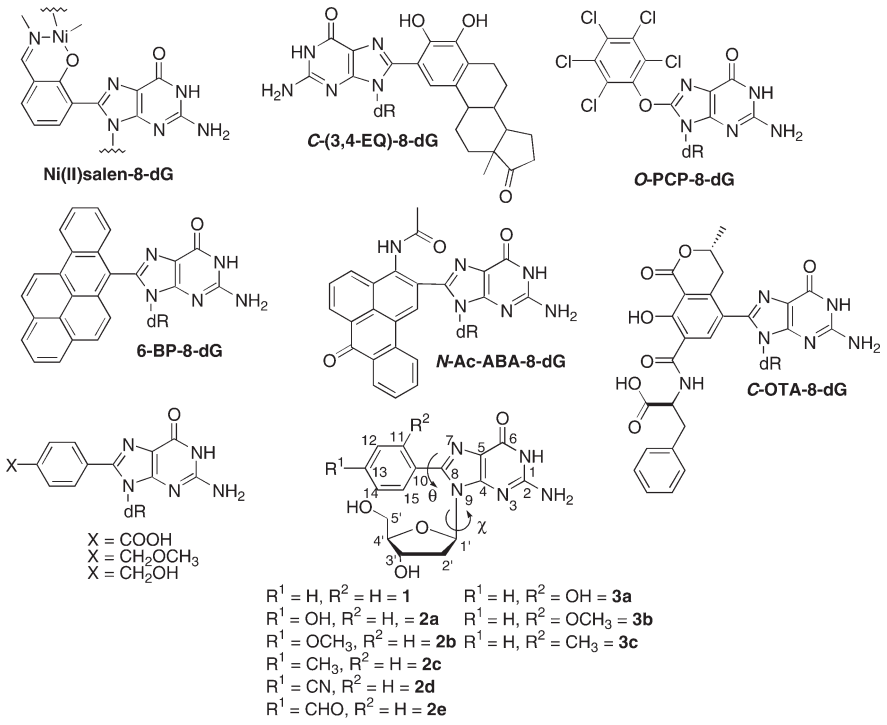

FIGURE 1. Examples of C^8-aryl adducts and the structure, atomic numbering, and identification of dihedral angles χ ($\angle(OC1'N_9C_4)$) and θ ($\angle(C_{11}C_{10}C_8N_9)$) for C^8-aryl adducts **1**−**3c**.

accompany C^8-aryl adduction in duplex DNA at physiological pH.

Results and Discussion

Structural Features of C^8-Aryl Adducts. Insight into the structural features of the C^8-aryl adducts was obtained from DFT calculations, as previously presented for the phenolic adducts **2a** (R^1 = OH) and **3a** (R^2 = OH).[27] Conformations for the other adducts were identified by reoptimizing the previously identified minima for the isomeric phenolic adducts with the OH substituent replaced with each R^1 or R^2 group. Representative DFT structures for an *anti*, *syn* and deglyco adduct are shown in Figure 2 for **3a** (R^2 = OH) and deglyco**3a** with N^9H. As noted for **2a** and **3a**,[27] *anti* structures are less stable than *syn* structures by ~25 kJ mol^{-1} for all C^8-aryl-dG adducts **1**−**3c**. This preference is consistent with the known structural preference of C^8-*p*-NMe_2-Ph-guanosine, which adopts a *syn* conformation in both the solid state and solution.[28] For **1**−**3c**, all *syn* minima contain a strong $O^{5'}$−H···N^3 hydrogen bond (1.80−1.96 Å), and the aryl substituent is twisted with respect to the nucleobase, where the magnitude of the twist angle (θ) depends on steric considerations and favorable intramolecular interactions. For example, the global minima for *p*-adducts **1**−**2e** are twisted by ~37°, while θ increases to 45° for **3c** (R^2 = CH_3) and 55° for **3b** (R^2 = OCH_3) due to steric interactions between R^2 and the nucleobase. In contrast, the **3a** (R^2 = OH) global minimum is less twisted (θ = 27°) than any other substituent due to O−H···N^7 hydrogen bonding.[27]

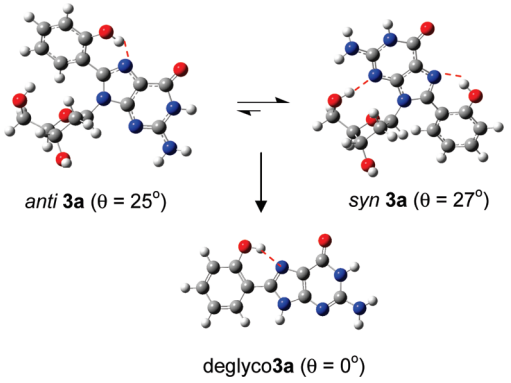

FIGURE 2. Global *anti*,*syn* and deglyco minima for **3a** fully optimized with B3LYP/6-31G(d), highlighting twist angles (θ, deg) and hydrogen-bonding interactions (dashed red lines). The *syn* minimum is favored over *anti* by ~25 kJ mol^{-1}.

For adducts **1**−**3b**, the neutral nucleobase global minima are planar (θ = 0°), suggesting that the sugar moiety is inducing the twist within the nucleobase.[27] It is also important to point out that the barrier to rotation is greater for the deglyco adducts than the nucleoside adducts, implying that the sugar also increases conformational flexibility.[27] The lone exception to this trend is adduct **3c** ($R^2 = CH_3$), where deglyco**3c** remains significantly twisted (θ = 24°).

Absorbance spectra for adducts **1**−**3c** were initially recorded in aqueous pH 4 buffer (0.05 M citrate) at room temperature. Under these conditions, adducts were relatively stable, and distinct absorbance changes were noted upon removal of the deoxyribose sugar moiety. The spectrum recorded for **3a** (Figure 3a, spectrum i) was representative of spectra for adducts **1**, **2a**−**2c**, and **3b**, which all showed a

(27) Millen, A. L.; McLaughlin, C. K.; Sun, K. M.; Manderville, R. A.; Wetmore, S. D. *J. Phys. Chem. A* **2008**, *112*, 3742–3753.
(28) Sessler, J. L.; Sathiosatham, M.; Doerr, K.; Lynch, V.; Abboud, K. A. *Angew. Chem., Int. Ed.* **2000**, *39*, 1300–1303.

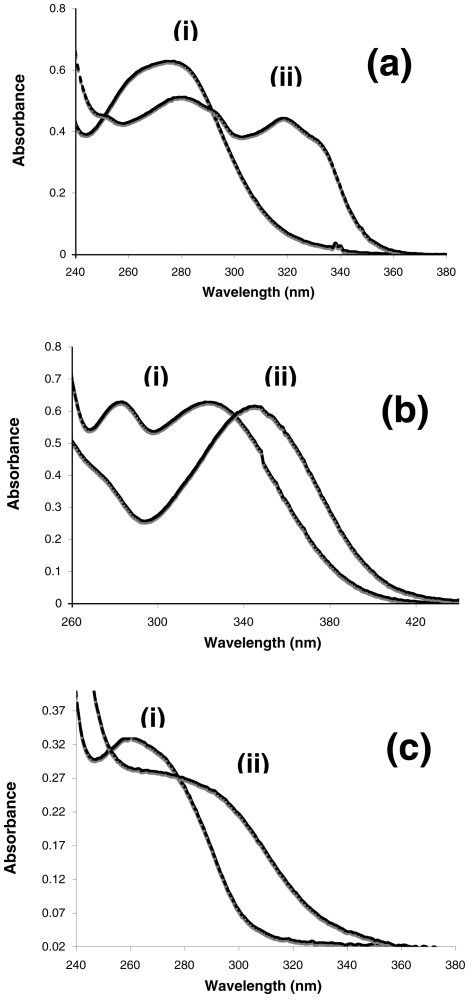

FIGURE 3. Absorbance spectra for a 50 μM solution of (a) (i) **3a** and (ii) deglyco**3a**, (b) (i) **2e** and (ii) deglyco**2e**, and (c) (i) **3c** and (ii) deglyco**3c** in 0.05 M citrate buffer, pH 4, μ = 0.31 M NaCl.

single broad peak at approximately 280 nm that exhibits a red shift compared to λ_{max} for dG at ~253 nm.[29] The adduct deglyco**3a** (Figure 3a, spectrum ii) showed two maxima at 290 and 318 nm, with the 318 nm absorbance being consistent with a planar deglyco**3a** structure with increased conjugation. The *p*-adducts **2d** (R^1 = CN) and **2e** (R^1 = CHO) bearing electron-withdrawing groups showed similar features. In pH 4 buffer, adduct **2e** showed two maxima at 282 and 323 nm (Figure 3b, spectrum i), while deglyco**2e** showed a single peak at ~350 nm (Figure 3b, spectrum ii). For **3c**, bearing the *o*-CH_3 substituent (Figure 3b, spectrum i), a single peak at ~261 nm was observed of weaker intensity and blue-shifted compared to all other adduct absorbances. The deglyco**3c** adduct (Figure 3b, spectrum ii) showed a broad absorbance with λ_{max} = 285 nm, which was also significantly blue-shifted compared to the absorbance for the other deglycosylated adducts. The UV−vis parameters and structural features of adducts **1**−**3c** are summarized in Table 1.

Proton Affinity. Ionization constants for the C^8-aryl-dG adducts in the low pH region (1−4) were determined using

(29) Onidas, D.; Markovitsi, D.; Marguet, S.; Sharonov, A.; Gustavsson, T. *J. Phys. Chem. B* **2002**, *106*, 11367–11374.

TABLE 1. UV−vis Parameters and Structural Features[a] for Adducts 1−3c and Their Deglyco Analogues

adduct	λ_{max}, log ε[c]	θ (deg)	C_8-C_{10} (Å)
1 (R^1 = H)	277, 4.33	37.5	1.473
deglyco**1**[b]	305, 4.28	0.6	1.464
2a (R^1 = OH)	277, 4.36	37.0	1.471
deglyco**2a**	309, 4.35	0.6	1.463
2b (R^1 = OCH_3)	276, 4.34	37.4	1.471
deglyco**2b**	310, 4.45	0.6	1.463
2c (R^1 = CH_3)	277, 4.38	37.2	1.472
deglyco**2c**	308, 4.15	0.2	1.463
2d (R^1 = CN)	311, 4.09	38.0	1.470
deglyco**2d**	334, 3.92	0.1	1.460
2e (R^1 = CHO)	323, 4.12	38.1	1.471
deglyco**2e**	350, 4.07	0.5	1.460
3a (R^2 = OH)	275, 4.10	27.0	1.464
deglyco**3a**	318, 3.95	0.0	1.455
3b (R^2 = OCH_3)	278, 4.25	55.3	1.477
deglyco**3b**	319, 4.04	0.0	1.466
3c (R^2 = CH_3)	261, 3.78	45.3	1.477
deglyco**3c**	285, 3.70	24.0	1.468
dG	252.7, 4.14[d]		

[a]Structures were fully optimized with B3LYP/6-31G(d), and relative energies were obtained from B3LYP/6-311+G(2df,p) single-point calculations. [b]Calculations for deglyco adducts with N^9H. [c]Determined in 0.05 M citrate buffer pH 4, μ = 0.31 M NaCl. [d]Taken from ref 29.

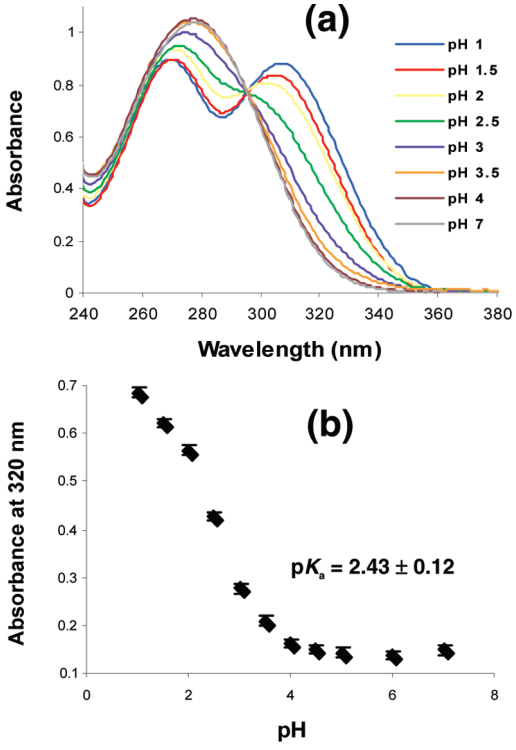

FIGURE 4. (a) Overlay spectra for **2a** as a function of pH at 20 °C. (b) Initial absorbance at 320 nm vs pH for **2a**.

the spectrophotometric procedure at 20 °C, as outlined previously for C^8-(arylamino)-dG adducts.[23] Figure 4a shows overlay absorbance spectra for adduct **2a** (R^1 = OH) as a function of pH at 20 °C, while shown in Figure 4b is a plot of initial absorbance at 320 nm vs pH from the absorbance data shown in Figure 4a. The spectrophotometrically determined pK_{a1} for **2a** (2.43 ± 0.12) is in the range expected for pK_{a1} of dG; for example, a recent pK_{a1}

TABLE 2. Gas-Phase Proton Affinities (PA), Ionization Constants, and Structural Features[a] for Adducts 1−3c Protonated at N^7 (N^7H^+)

adduct	PA[b]	pK_a	θ (N^7H^+)	$\Delta\theta$ [g]	C_8-C_{10} (N^7H^+)	Δ C_8-C_{10}[h]
1 (R^1 = H)	230.0	2.41 ± 0.04[d]	42.3	4.8	1.462	−0.011
2a (R^1 = OH)	231.7	2.43 ± 0.12[d]	42.8	5.8	1.454	−0.017
2b (R^1 = OCH_3)	233.1	2.48 ± 0.06[d]	42.1	4.7	1.453	−0.018
2c (R^1 = CH_3)	231.8	2.41 ± 0.12[d]	40.7	3.5	1.459	−0.013
2d (R^1 = CN)	222.7	2.00[e]	42.0	4.0	1.464	−0.006
2e (R^1 = CHO)	225.2	2.12[e]	42.3	4.2	1.464	−0.007
3a (R^2 = OH)	226.9	2.21 ± 0.17[d]	28.3	1.3	1.457	−0.007
3b (R^2 = OCH_3)	234.1	2.57 ± 0.26[d]	28.8	−26.5	1.456	−0.021
3c (R^2 = CH_3)	231.7	2.40 ± 0.22[d]	68.2	22.9	1.471	−0.006
dG	232.0 (234.4)[c]	2.34[f]				

[a]Structures were fully optimized with B3LYP/6-31G(d) (relative energies from B3LYP/6-311 + G(2df,p) single-point calculations). [b]N^7 proton affinity (PA) in the gas phase calculated as the negative of the enthalpy change for protonation (kcal mol^{-1}). [c]Experimental PA for dG taken from ref 30. [d]Obtained from spectrophotometric titration at 20 °C. [e]Estimated from gas-phase N^7 PA and experimentally determined pK_a values. [f]Taken from ref 17. [g]$\Delta\theta = \theta(N^7H^+) - \theta$(neutral adduct). [h]$\Delta C_8-C_{10} = C_8-C_{10}$ (N^7-H^+) − C_8-C_{10} (neutral adduct).

value for N^7-protonated dG is 2.34.[17] The pK_{a1} value for **2a** was similar to the values determined for the other *p*-substituted adducts **1**−**2c**, which all exhibited a red shift upon protonation and gave a narrow pK_{a1} range (2.41−2.48), as reported in Table 2. Variation in pK_{a1} was observed for *o*-substituted analogues **3a** (R^2 = OH) and **3b** (R^2 = OCH_3). Compared to the *p*-substituted analogues, **3a** exhibited a decrease in pK_{a1} (2.21 ± 0.17), while **3b** showed an increase (2.57 ± 0.26).

Also reported in Table 2 are the calculated gas-phase proton affinity (PA) values for the most basic N^7-site of adducts **1**−**3c**. For **1**, the N^7 PA is 230.0 kcal mol^{-1}, which is similar to the calculated N^7 PA for dG (232 kcal mol^{-1}) as well as the experimental PA for dG (234.4 kcal mol^{-1}).[30] The N^7 PA values for **1**−**3c** lie within a narrow range (222.7−234.1 kcal mol^{-1}) with the lowest value for **2d** (R^1 = CN) and the highest value for **3b** (R^2 = OCH_3). A plot of N^7 PA vs spectrophotometrically determined pK_{a1} values affords a straight line, from which pK_{a1} values for **2d** and **2e** were estimated. Even though the data reported in Table 2 support protonation at N^7, it has been speculated that C^8-substituents may differentially stabilize protonation at N^3 rather than N^7.[23] However, this seems unlikely given that N^7-protonation is much more favorable energetically than N^3-protonation for dG (PA for N^3 of dG is 220.1 kcal mol^{-1})[31] and that protonation of 8-oxoguanine occurs at N^3 with pK_{a1} of 0.22.[32]

Table 2 also reports changes in the twist (θ) angle and C^8-C^{10} bond length upon N^7-protonation. For the *p*-substituted adducts **1**−**2e**, the optimized protonated structures were not greatly altered from the neutral structures. The global minima are in the same *syn* conformation with a strong $O^{5\prime}-H\cdots N^3$ hydrogen bond, and the *anti* structures are higher in energy (by ∼19 kJ mol^{-1}). The N^7-protonated *p*-adducts are more twisted than the neutral species (by about 3−6°) due to increased steric interactions between the aryl ring and the protonated nucleobase. Despite the increase in twist angle (θ), the N^7-protonated nucleosides have shorter C^8-C^{10} bonds, especially when R^1 is electron-donating (OH, OCH_3). The *o*-substituted adducts **3a**−**c** behave differently upon N^7-protonation. Adduct **3a** (R^2 = OH) shows only a small 1.3° increase in θ due to $O-H\cdots N^7$ hydrogen-bonding interactions involving the phenolic group in both the neutral and protonated adduct. The relatively low pK_{a1} value for **3a** suggests preferential hydrogen bonding in the neutral adduct, with a concomitant decrease in N^7 PA.[30] In contrast, adduct **3b** (R^2 = OCH_3) becomes much less twisted (by 27.2°) upon N^7-protonation and has the same degree of twist as neutral **3a** due to $N^7-H\cdots O-CH_3$ hydrogen-bonding. This preferential stabilization of the N^7-protonated adduct for **3b** is also reflected in the relatively large decrease in the C^8-C^{10} bond length and the increase in pK_{a1}. For **3c** (R^2 = CH_3), the N^7-protonated adduct is significantly more twisted (22.9°) than the neutral species due to increased sterics. Overall, the calculations and spectrophotometrically determined pK_{a1} values support N^7-protonation for C^8-aryl-dG adducts **1**−**3c**.

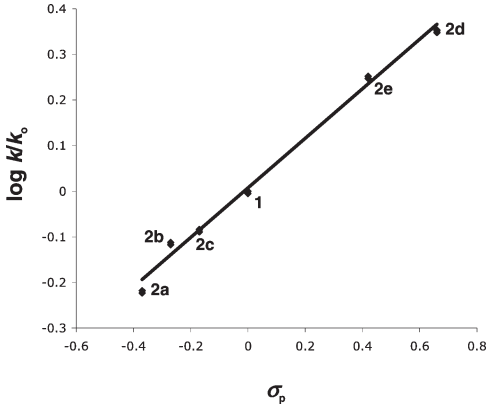

FIGURE 5. Hammett plot for adducts **1**−**2e** using σ_p vs log k/k_o in 0.1 M HCl at 37.2 °C.

Rates of Hydrolysis. First-order rate constants were determined spectrophotometrically by monitoring formation of the deglycosylated product at its absorbance maximum. Apparent first-order rate constants, k (min^{-1}), and half-lives, $t_{1/2}$ (min), were first determined for the hydrolysis of adducts **1**−**3c** in 0.1 M HCl at 37.2 °C and 0.05 M pH 4 citrate buffer at 48.4 °C, with ionic strength maintained at μ = 0.31 M NaCl. These particular conditions were chosen in order to draw direct comparison to hydrolysis rates of dG.[16b] Figure 5 shows a plot of log k/k_o versus Hammett σ_p for hydrolysis of *p*-adducts **1**−**2e** in 0.1 M HCl at 37.2 °C. A linear correlation with a small positive slope (ρ) of 0.543 was observed, implying an increase in rate by electron-withdrawing groups and that the hydrolysis is less sensitive than benzoic acid dissociation to the electronic nature of the *p*-substituent.

(30) Greco, F.; Liguori, A.; Sindona, G.; Uccella, N. *J. Am. Chem. Soc.* **1990**, *112*, 9092–9096.
(31) Xia, F.; Xie, H.; Cao, Z. *Internat. J. Quantum Chem.* **2008**, *108*, 57–65.
(32) Jang, Y. H.; Goddard, W. A. III; Noyes, K. T.; Sowers, L. C.; Hwang, S.; Chung, D. S. *Chem. Res. Toxicol.* **2002**, *15*, 1023–1035.

TABLE 3. Summary of First-Order Rate Constants, k (min^{-1}), and Half-Lives, $t_{1/2}$ (min), for Hydrolysis of Adducts 1−3c in HCl and pH 4 Buffer at 37 and 48 °C

adduct	k_{obs}(HCl), $t_{1/2}$[a]	k_{obs}/k_{obs} (dG)	k_{obs} (pH 4), $t_{1/2}$[c]	k_1 (pH 4)[d]	k_1/k_1 (dG)	$\Delta\theta$[e]	$\Delta C_8{-}C_{10}$[f]
1 (R^1 = H)	0.790 ± 0.008, 0.877	20.2	(2.61 ± 0.08) × 10^{-2}, 26.6	1.015	92.3	−42.3	0.002
2a (R^1 = OH)	0.478 ± 0.009, 1.45	12.2	(3.1 ± 0.1) × 10^{-2}, 22	1.152	104.7	−42.6	0.009
2b (R^1 = OCH_3)	0.611 ± 0.006, 1.13	15.6	(2.95 ± 0.09) × 10^{-2}, 23.5	0.977	88.8	−42.0	0.010
2c (R^1 = CH_3)	0.651 ± 0.009, 1.06	16.6	(2.84 ± 0.08) × 10^{-2}, 24.4	1.105	100.5	−39.8	0.004
2d (R^1 = CN)	1.78 ± 0.02, 0.389	45.5	(2.3 ± 0.1) × 10^{-2}, 30	2.300	209.1	−42.0	−0.004
2e (R^1 = CHO)	1.41 ± 0.01, 0.491	36.1	(2.38 ± 0.07) × 10^{-2}, 29.1	1.805	164.1	−42.1	−0.004
3a (R^2 = OH)	0.282 ± 0.001, 2.46	7.2	(1.06 ± 0.02) × 10^{-2}, 65.4	0.654	59.5	−28.3	−0.002
3b (R^2 = OCH_3)	0.291 ± 0.003, 2.38	7.4	(7.4 ± 0.2) × 10^{-3}, 94	0.199	18.1	−28.8	0.010
3c (R^2 = CH_3)	0.196 ± 0.002, 3.45	5.0	(2.6 ± 0.2) × 10^{-3}, 270	0.103	9.4	−39.2	−0.003
dG	0.0391, 17.7[b]		2.44 × 10^{-4}, 2840[b]	0.011			

[a]Determined in 0.1 M HCl at 37.2 °C. [b]Taken from ref 16b. [c]Determined in 0.05 M citrate buffer pH 4, μ = 0.31 M NaCl at 48.4 °C. [d]$k_1 \approx k_{obs}K_{a1}/[H^+]$. [e]$\Delta\theta$ = θ (N^7H^+ adduct) − θ (neutral nucleobase with N^7H). [f]Δ $C_8{-}C_{10}$ = $C_8{-}C_{10}$ (N^7H^+ adduct) − $C_8{-}C_{10}$ (neutral nucleobase).

For comparison to dG, the C^8-aryl adduct 8-Ph-dG (**1**), which bears no substituent, underwent deglycosylation ~20 times faster than dG in 0.1 M HCl. This behavior was contrasted by adducts **3a**−**c** with *o*-substituents that underwent hydrolysis at a significantly slower rate than their *p*-substituent counterparts in 0.1 M HCl. In particular, 8-*o*-CH_3Ph-dG (**3c**) underwent hydrolysis ~3 times slower than 8-*p*-CH_3Ph-dG (**2c**) in 0.1 M HCl and only showed a 5-fold increase in rate compared to dG.

For the rate data obtained at pH 4, the pK_{a1} values reported in Table 2 were used to estimate k_1 for the rate-limiting C−N bond cleavage from the N^7-protonated adducts **1**−**3c**. As reported previously for acid-catalyzed hydrolysis of dG-[16] and C^8-substituted dG analogues,[23] both the monoprotonated and diprotonated substrates are subject to rate-limiting C−N bond cleavage. The pK_{a2} for the diprotonated substrate is ca. −2.5,[16c] and the C^8-substituent is expected to have little effect on K_{a2}.[23] At pH 4, where involvement of the diprotonated species can be ignored, the rate expression simplifies to $k_{obs} = k_H a_H$, where $k_H \approx k_1/K_{a1}$. Thus, at pH 4, $k_1 \approx k_{obs}K_{a1}/[H^+]$, and k_1 values for **1**−**3c** are given in Table 3. The C^8-aryl substituent clearly increases the magnitude of k_1 relative to k_1 for dG. The effects for the *p*-adducts **1**−**2e** are ca. 90- to 200-fold larger than k_1 for dG, while the effects for the *o*-adducts **3a**−**c** are only ca. 9- to 60-fold larger. For comparison, C^8-arylamino substituents increase k_1 by ca. 3- to 15-fold,[23] which is similar to the rate enhancement exerted by the least reactive C^8-aryl-dG adduct **3c** (R^2 = CH_3).

The observed decrease in the rate of hydrolysis for the *o*-adducts **3a**−**c** compared to the *p*-adducts **1**−**2e** was somewhat surprising given that a bulky substituent at C^8 is expected to increase the rate of hydrolysis due to the relief of strain in the activated complex in an A-1 mechanism.[24] However, a rationale for the decrease in rates of hydrolysis for **3a**−**c** relative to **1**−**2e** is provided by considering the changes in the twist angle (θ) and $C^8{-}C^{10}$ bond length (Table 3) when going from the N^7-protonated nucleoside adduct to the neutral nucleobase with N^7H that lacks the sugar moiety (Figure 6). It is important to point out that the twist angle (θ) for the N^7H nucleobase intermediate differs slightly from the N^9H nucleobase shown in Figure 2 with θ values given in Table 1 for the deglyco adducts. For the *p*-adducts **1**−**2e**, a decrease in twist angle of ca. 40° is observed upon removal of the sugar group from the twisted N^7-protonated species to form the planar nucleobase. For **2d** and **2e**, which bear electron-withdrawing groups, the

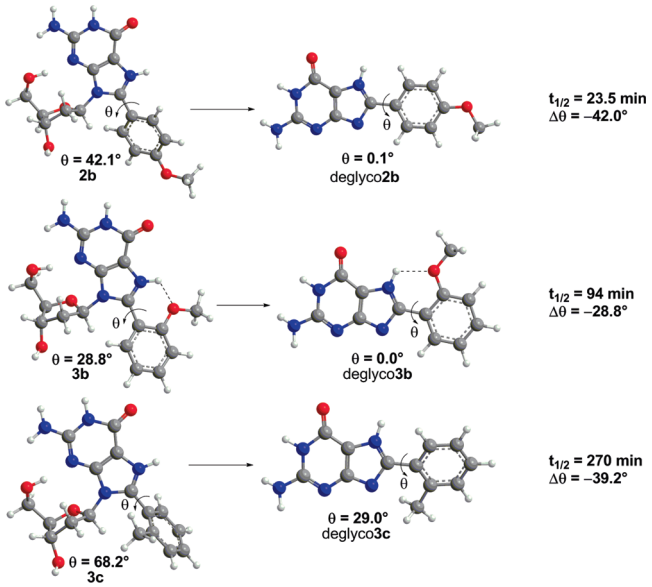

FIGURE 6. Structural changes in the nucleobase upon deglycosylation for **2b**, **3b**, and **3c**.

$C^8{-}C^{10}$ bond length also shortens, suggesting preferential stabilization of the neutral nucleobase compared to the protonated nucleoside. This phenomenon would also be expected to increase the rate of hydrolysis.

For *o*-adducts **3a** and **3b**, the decrease in twist angle upon sugar removal to form the planar nucleobase is only ca. 28° because the N^7-protonated nucleoside is relatively planar due to hydrogen-bonding interactions between the R^2 substituent and N^7H^+. Thus, the relief in strain for **3a** and **3b** upon sugar removal is not as great as it is for **1**−**2e**, and hence, the rate of hydrolysis is diminished. Differentiation between **3a** and **3b** is apparent from the $C^8{-}C^{10}$ bond length changes, where the bond becomes shorter for **3a** and longer for **3b**. This suggests preferential stabilization of the neutral nucleobase for **3a**, and hence, its rate of hydrolysis is greater than the rate for **3b**. For **3c**, which bears the *o*-CH_3 substituent, the change in twist of 39° suggests considerable relief of strain. However, in this case, unlike the other C^8-aryl-G adducts, the neutral nucleobase is not planar, but has a twist angle θ of 29° (Figure 6). This suggests that the nucleobase is also sterically hindered and that the relief of strain for **3c** upon sugar removal is diminished due to hindrance in the free nucleobase.

TABLE 4. Summary of First-Order Rate Constants, k (min^{-1}), and Half-Lives, $t_{1/2}$ (min), for Hydrolysis of Adducts 1, 2a, 2e, and 3c at 37 °C

adduct	pH 1 k, $t_{1/2}$[a]	pH 2 k, $t_{1/2}$[b]	pH 3 k, $t_{1/2}$[b]	pH 4 k, $t_{1/2}$[b]	pH 7 k, $t_{1/2}$ (days)[c]
1	1.36 ± 0.08, 0.510	0.300 ± 0.006, 2.31	0.0591 ± 0.0005, 11.7	0.0041 ± 0.0001, 170	1.90×10^{-5}, 25
2a	0.95 ± 0.02, 0.73	0.217 ± 0.004, 3.19	0.0424 ± 0.0005, 16.3	0.0055 ± 0.0001, 125	3.80×10^{-5}, 13
2e	4.6 ± 0.1, 0.15	0.504 ± 0.007, 1.36	0.046 ± 0.003, 15	0.0043 ± 0.0001, 160	4.06×10^{-6}, 118
3c	0.37 ± 0.03, 1.9	0.047 ± 0.002, 15	0.0054 ± 0.0005, 130	0.0004 ± 0.0001, 1730	5.20×10^{-7}, 924

[a]Determined in 0.05 M phosphate buffer, μ = 0.31 M NaCl. [b]Determined in 0.05 M citrate buffer, μ = 0.31 M NaCl. [c]Estimated rate data based on first-order dependence on H^+ activity.

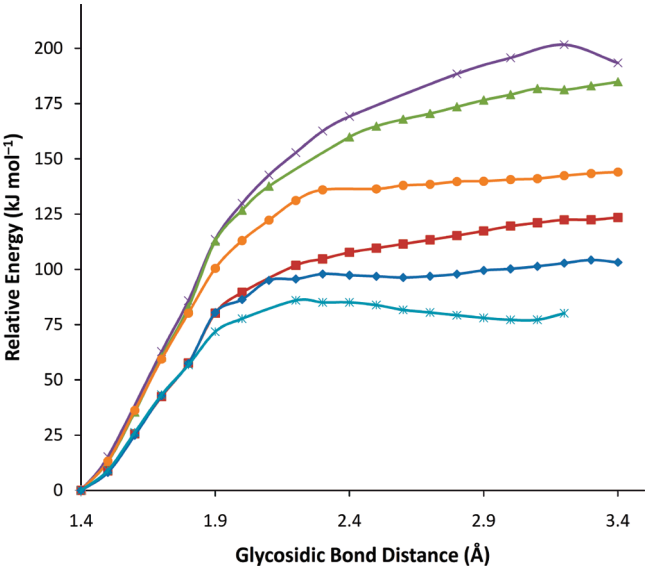

FIGURE 7. Deglycosylation profile calculated with constrained PCM-B3LYP/6-31G(d) optimizations for *anti* (×, purple) and *syn* (△, green) neutral dG, *anti* (□, red) and *syn* (◇, dark blue) N^7H^+ dG, and neutral (○, orange) and N^7H^+ (*, light blue) *syn*-**1**.

The effects of the structural changes in the modified base on the rates of deglycosylation can be further broken down and analyzed through consideration of experimentally determined activation parameters and DFT calculations of the energetic effects of extending the glycosyl bond (Figure 7). For dG, previously reported activation parameters determined in 0.1 M HCl are as follows: $\Delta H^{\ddagger}$ = 22.5 kcal mol^{-1} (94.2 kJ mol^{-1}); $\Delta S^{\ddagger}$ = 4.3 cal mol^{-1} K^{-1}; and $\Delta G^{\ddagger}$ = 21.2 kcal mol^{-1} (88.7 kJ mol^{-1}).[16b] For comparison, the corresponding parameters for C^8-Ph-dG (**1**) ($\Delta H^{\ddagger}$ = 19.7 kcal mol^{-1} (82.5 kJ mol^{-1}); $\Delta S^{\ddagger}$ = 4.5 cal mol^{-1} K^{-1}; $\Delta G^{\ddagger}$ = 18.4 kcal mol^{-1} (77.0 kJ mol^{-1}) were determined in 0.1 M HCl at six different temperatures ranging from 25 to 60 °C to allow generation of an Eyring plot (data not shown). This indicates that attachment of the C^8-phenyl substituent lowers the C−N cleavage barrier by ~12 kJ mol^{-1}.

Dissection of the structural features that account for this decrease in barrier height is provided by inspection of the calculated deglycosylation profile for dG vs **1** shown in Figure 7. By estimating the barriers from the energetic plateaus, it can be seen that although natural dG prefers the *anti* conformation over *syn* by ~11 kJ mol^{-1}, the barrier to deglycosylation of the *syn* conformer (~175 kJ mol^{-1}) is ~20 kJ mol^{-1} less than the corresponding barrier for *anti* (~195 kJ mol^{-1}). Therefore, the *syn* orientation induced by the bulky C^8-substituent may contribute to the acceleration of the hydrolysis rates of C^8-aryl adducts. Nevertheless, when the barrier of neutral *syn* dG is compared to neutral C^8-Ph-dG (**1**), a large effect (~ 40 kJ mol^{-1}) of the bulky C^8-Ph group is still observed (green vs orange line in Figure 7). Interestingly, N^7-protonation has a larger (80 kJ mol^{-1}, purple vs red line) effect on the barrier for dG deglycosylation than it does for C^8-Ph-dG (50 kJ mol^{-1}, orange vs light blue line). This diminishes the role of the C^8-phenyl substituent in acidic media where N^7 is protonated, although the calculations correctly predict that N^7H^+ **1** still has the lowest barrier for C−N cleavage overall (by ~20 kJ mol^{-1}). This role of pH on the relative rates of deglycosylation of modified dG bases vs natural dG is noted in the rate data presented in Table 3 where k_{obs}(**1**)/k_{obs}dG is 20 in 0.1 M HCl and ~100 at pH 4. The same phenomenon was observed for the hydrolysis of C^8-arylamine adducts that exhibited considerably higher rates of hydrolysis than dG at pH ~3−7 but became comparable (within a factor of 5) at pH < 2.[23]

Hydrolysis at Physiological pH. Hydrolysis kinetics between pH 1−4 for C^8-aryl-dG adducts **1**, **2a**, **2e**, and **3c** at 37 °C yielded straight lines, as observed for dG[16,23] and other purine nucleosides.[33] This has been interpreted to mean that $k_1/K_{a1} \approx k_2/K_{a2}$[16,23,33] and that the hydrolysis reaction shows a continuous first-order dependence on H^+ activity.[16] This permitted extrapolation of the rate data to pH 7 for an estimate of hydrolysis rates at physiological pH (Table 4). For C^8-Ph-dG (**1**), a first-order rate constant of 1.90×10^{-5} min^{-1}, with $t_{1/2}$ = 25 days, was determined at pH 7. For comparison, a rate for spontaneous loss of purines from duplex DNA at pH 7.4 at 37 °C is ~3×10^{-11} s^{-1} ($t_{1/2}$ = 730 years).[34] Thus, while C^8-aryl-dG adducts are significantly more reactive than dG toward hydrolysis, they are reasonably stable at physiological pH and should be even more stable within duplex DNA where purines are more resistant to hydrolysis.[18] The hydrolysis kinetics for C^8-aryl-dG adducts **1**−**3c** suggests that these adducts are unlikely to be intermediates prior to loss of the deoxyribose sugar and that an alternative explanation accounts for the accompaniment of abasic site formation during C^8-aryl-purine formation at physiological pH.

Rationale for Abasic Site Formation. Insight into the cause of abasic site formation during C^8-aryl-purine adduction is provided by recent studies from the Kenttämaa laboratory on reactions of phenyl radicals toward nucleic acids in the gas phase.[35] These studies employ mass spectrometry coupled with laser-induced acoustic desorption (LIAD) to examine the reactivity of phenyl radicals with dinucleoside phosphates in the gas phase. Both H-atom abstraction from the sugar moiety and direct radical addition to the C^8-site of

(33) Oivanen, M.; Lönnberg, H.; Zhou, X.-X.; Chattopadhyaya, J. *Tetrahedron* **1987**, *43*, 1133–1140.
(34) Lindahl, T.; Karlstrom, O. *Biochemistry* **1973**, *12*, 5151–5154.
(35) (a) Ramirez-Arizmendi, L. E.; Heidbrink, J. L.; Guler, L. P.; Kenttämaa, H. I. *J. Am. Chem. Soc.* **2003**, *125*, 2272–2281. (b) Liu, J.; Petzold, C. J.; Ramirez-Arizmendi, L. E.; Perez, J.; Kenttämaa, H. I. *J. Am. Chem. Soc.* **2005**, *127*, 12758–12759. (c) Yang, L.; Nash, J. J.; Yurkovich, M. J.; Jin, Z.; Vinueza, N. R.; Kenttämaa, H. I. *Org. Lett.* **2008**, *10*, 1889–1892.

SCHEME 1. Proposed Pathways for the Degradation of the Nucleoside Radical Intermediate Following Phenyl Radical Attachment at C^8-dG

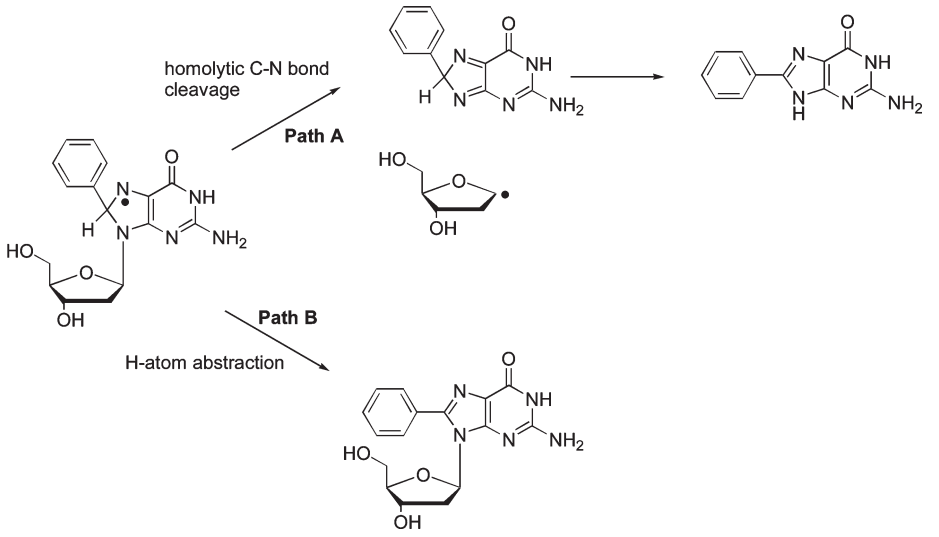

purine bases are observed,[35] as noted for the reactivity of phenyl radicals toward DNA in solution.[15,36] Interestingly, the radical addition reaction at C^8 of purines is always followed by C−N bond cleavage with formation of the nucleobase lacking the sugar moiety.[35] Thus, as outlined in Scheme 1, direct phenyl radical attachment at C^8-dG generates the resonance-stabilized radical nucleoside intermediate. In path A, the radical intermediate undergoes homolytic C−N bond cleavage to eliminate the free base, as observed in the gas phase for addition of the phenyl radical to C^8 of purines.[35] H-atom abstraction to form the stable nucleoside adduct in path B would be a competitive process to path A. In the gas phase, path B cannot compete with path A and so only homolytic C−N bond cleavage is observed.[35] However, path B would be expected to compete with path A in water. As a model for path B, it is known that the resonance-stabilized cyclohexadienyl radical undergoes very rapid H-atom transfer with molecular oxygen with a second order rate of 1.64×10^9 M^{-1} s^{-1} in benzene and that this reaction shows essentially no dependence on solvent polarizability, polarity and ability to hydrogen bond.[36] Assuming an oxygen concentration of 1.2 mM for an O_2-saturated solution,[37] a first-order rate of $\sim 2 \times 10^6$ s^{-1} for path B can be estimated. This suggests a similar rate for the homolytic C−N bond cleavage in path A given that significant levels of abasic site formation accompany C^8-aryl-purine adduction;[12,15]the C1′-radical would be expected to form the oxidized abasic site 2-deoxyribonolactone in the presence of O_2 and water.[38] Thus, oxygen is likely to promote C^8-dG adduct formation in solution by providing a rapid and productive path for aromatization of the nucleoside radical intermediate.[39] Experiments are currently underway to test this hypothesis.

Conclusions

The current study has allowed us to conclude the following: (1) C^8-aryl-dG nucleoside adducts adopt a *syn* conformation containing a strong $O^{5\prime}-H\cdots N^3$ hydrogen bond with the aryl ring twisted with respect to the nucleobase. In general, removal of the deoxyribose sugar moiety affords a planar nucleobase adduct that exhibits a red shift compared to λ_{max} for the nucleoside adduct. These adducts undergo protonation at N^7 with ionization constants and calculated N^7 proton affinity (PA) values that are similar to those measured for dG. (2) C^8-aryl-dG nucleoside adducts are more prone than dG to acid-catalyzed hydrolysis. C^8-aryl-dG adducts **1**−**2e** that bear para substituents have k_1 values that are ca. 90- to 200-fold larger than k_1 for dG, while the effects for the ortho adducts **3a**−**c** are only ca. 9- to 60-fold larger. Relief of steric strain upon removal of the deoxyribose sugar moiety provides a rationale for this relative reactivity. Calculated deglycosylation pathways show that protonation at N^7, the bulky substituent, and the *syn* orientation all contribute to the increase in the rate of C−N glycosidic bond cleavage. (3) Despite the enhanced reactivity of these bases in acid compared to dG, they are relatively stable at physiological pH with $t_{1/2} \sim 25$ days. Given that abasic site formation is known to accompany C^8-aryl-dG adduct formation, our results suggest that these nucleoside adducts are unlikely intermediates leading to abasic site formation at physiological pH. Instead, a resonance-stabilized, radical nucleoside intermediate that forms upon direct radical attachment at the C^8-site of purines, and is a known precursor to C^8-aryl-dG adduction following H-atom abstraction, is the more likely intermediate leading to the elimination of the nucleobase by homolytic C−N bond cleavage.

Experimental Section

Suzuki Coupling of 8-Br-dG with Boronic Acids. These reactions were conducted according to the literature[25] and are briefly described here. Palladium acetate (2.2 mg, 0.01 mmol),

(36) Maillard, B.; Ingold, K. U.; Scaiano, J. C. *J. Am. Chem. Soc.* **1983**, *105*, 5095–5099.
(37) Linke, W. F. *Solubilities, Inorganic and Metalo Organic Compounds: A Compilation of Solubility Data from the Periodocal Literature*; Van Nostrand: Princeton, 1958−1965; p 1228.
(38) (a) Chatgilialoglu, C.; Ferreri, C.; Bazzanini, R.; Guerra, M.; Choi, S.-Y.; Emanuel, C. J.; Horner, J. H.; Newcomb, M. *J. Am. Chem. Soc.* **2000**, *122*, 9525–9533. (b) Huang, H.; Greenberg, M. M. *J. Org. Chem.* **2008**, *73*, 2695–2703.
(39) Curran, D. P.; Keller, A. I. *J. Am. Chem. Soc.* **2006**, *128*, 13706–13707.

tris(2-sulfophenyl)phosphine trisodium salt (TPPTS) (14.8 mg, 0.025 mmol), sodium carbonate (80 mg, 0.75 mmol), 8-Br-dG (0.375 mmol), and the appropriate boronic acid (0.45 mmol) were added to deoxygenated 2:1 water:acetonitrile (3.5 mL) and heated to 80 °C for 4 h under an argon balloon. The reaction was diluted with ca. 20 mL of water and the pH adjusted to 6−7 with 1 M HCl (aq). The mixture was allowed to cool to 0 °C for several hours before the product was recovered by vacuum filtration. Adducts **1**,[25a] **2a**−**e**,[25a,7b,7c] and **3a**,**b**[7a] were prepared as described and NMR spectra were identical to previously published spectra provided in Supporting Information.[7,25a] The corresponding guanine analogues of adducts **1**−**3c** were prepared, as previously outlined,[7a,27] by placing the adduct in ca. 20 mL of 10% formic acid under heat (75 °C) for 1 h. After cooling, the reaction mixtures were brought to pH 6 with 1 M NaOH, and products were recovered by crystallization and filtering from the aqueous media. The deglycosylated adducts were used as standards for spectroscopic measurements.

8-(2″-Tolyl)-2′-deoxyguanosine (3c). Starting from 8-Br-dG (0.504 g, 1.46 mmol), 2-tolylboronic acid (0.594 g, 4.37 mmol), $Pd(OAc)_2$ (32.8 mg, 0.146 mmol), TPPTS (0.144 g, 0.244 mmol), and Na_2CO_3 (0.312 g, 2.92 mmol), adduct **3c** was obtained as an off-white solid (65.7 mg, 13%) following purification by flash chromatography on silica (1:10 $MeOH/CH_2Cl_2$): ^1H NMR (DMSO-d_6) (300 MHz) δ 11.4 (s, 1H), 7.42−7.30 (m, 4H), 6.46 (s, 2H), 5.71 (m, 1H), 5.66 (brs, 1H), 5.10 (brs, 1H), 4.20 (m, 1H), 3.72 (m, 1H), 3.50−3.43 (m, 2H), 2.96 (m, 1H), 2.16 (s, 3H), 1.93 (m, 1H); ^{13}C NMR (DMSO-d_6) (75.5 MHz) δ 159.0, 154.8, 151.1, 145.5, 138.0, 130.6, 130.3, 130.2, 129.6, 125.6, 117.0, 87.8, 84.7, 71.3, 62.2, 37.1, 19.4; HRMS calcd for $C_{17}H_{18}N_5O_4$ $[M - H]^-$ 356.1359, found 356.1346.

Spectroscopic Measurements. Stock solutions of adducts were made in DMSO to a concentration of 4 mM. Spectroscopic solutions were prepared with 25 μL of stock solution and 1.975 mL of 0.1 M HCl, 0.05 M phosphate buffer (pH 1), or 0.05 M citrate buffer (pH 2, 3 and 4), with ionic strength (μ) maintained using 0.31 M NaCl. Absorbance scans were taken at 25 °C for spectroscopic solutions in 0.1 M HCl and 0.05 M phosphate buffer (pH 1) and at 37 °C for spectroscopic solutions in 0.05 M citrate buffer (pH 2, 3, and 4). Spectral measurements were observed from 220 to 400 nm, with a measurement obtained every 5 to 10 min. Spectroscopic measurements were made until deglycosylation was observed, and the absorbance maximum for the deglycosylated product was obtained.

pK_a Determination. N^7 pK_a values for C^8-Ph-dG adducts were determined spectrophotometrically at 20 °C. Solutions were prepared using 25 μL of 4 mM stock solution of the adduct in DMSO and 1.975 mL of 0.05 M phosphate buffer (pH 1 and 1.5), 0.05 M citrate buffer (pH 2, 2.5, 3, 3.5, 4, 4.5, 5), and 0.05 M MOPS buffer (pH 6 and 7). Spectral measurements were observed from 220 to 400 nm, with absorbance measurements obtained at pH values 1−7 and the initial absorbance recorded at 280 or 320 nm. pK_a values were obtained with the following equation: $pK_a = pH + \log[(A - A_M)/(A_I - A)]$ with A representing the initial absorbance at 280 or 320 nm, A_M representing absorption of the neutral species (pH 7), and A_I representing absorption of the protonated species (pH 1). pK_a values were determined at the pH values between 1.5 and 6, and the average was taken.

Kinetic Measurements. The first-order kinetics of hydrolysis was obtained spectrophotometrically at 37.2 or 48.4 °C. Solutions were prepared using 25 μL of 4 mM stock solution of the adduct in DMSO and 1.975 mL of 0.1 M HCl, 0.05 M phosphate buffer (pH 1) or 0.05 M citrate buffer (pH 2, 3, and 4). Kinetic runs were carried out in parallel using the multicell changer, with 6 kinetic runs obtained for each adduct in each set of conditions. The appearance of the deglycosylated product was monitored at its absorbance maximum, which was determined separately via a UV−vis absorbance scan as detailed above. Data points were recorded every 0.1 s until a plateau in the graphical fit could be observed. The first-order rate constants for the hydrolysis of adducts were obtained from plots of log [adduct] versus time and were linear to 4 half-lives.

DFT Calculations. The B3LYP/6-311+G(2df,p)//B3LYP/6-31G(d) potential energy surfaces of deglyco**1**-**3c** and their N7 protonated counterparts were considered as a function of θ, the dihedral angle that controls the relative orientation of the phenyl and nucleobase rings (Figure 1). For **1**−**3c**, the sugar puckering and the orientation of the nucleobase about the glycosidic bond (defined by the dihedral angle χ, Figure 1) must be considered in addition to rotation about θ in the corresponding adducts **1**−**3c**. Previously,[27] systematic B3LYP/6-31G(d) potential energy surface scans of **2a** and **3a** were performed where the dihedral angles referred to as χ and θ (Figure 1) were constrained in 10° increments from 0 to 360°. Preliminary conformational searches were performed using Monte Carlo with MMFF as implemented in the Spartan[40] software package to identify the preferred sugar conformation.[27] The ten lowest energy structures identified from these scans were subsequently optimized to a minimum with B3LYP/6-31G(d). For both **2a** and **3a**,[27] the lowest energy conformer involves C2′-endo sugar puckering, which is the puckering present in B-DNA. Additionally, the C5′ hydroxyl group is directed toward the nucleobase.[27] Finally, the C3′ hydroxyl group is directed toward C2′ ($\angle$(HC3′OH) is approximately −60°). To more accurately determine the geometries and relative energies of the minima and transition states identified from the potential energy surface scans for **2a** and **3a**, full optimizations (i.e., all constraints released) were subsequently performed.[27]

All minima identified for **2a** and **3a** were subsequently reoptimized with different R^1 and R^2 substituents to generate all adducts **1**−**3c**. Additional Monte Carlo calculations were performed on these adducts to ensure that lower energy minima were not missed. Subsequently, each minimum structure was protonated at N^7 and reoptimized to study the effects of an acidic environment on the adduct structure. The proton affinities were calculated in the gas phase as the negative of the enthalpy change,[30] for the reaction with the global minimum of the N7-protonated species as the product and the global minimum of the neutral species as the reactant. Higher level (B3LYP/6-311+G(2df,p)) single-point calculations as well as B3LYP/6-31G(d) frequency calculations were performed in the gas phase on all fully optimized structures with zero-point vibrational energies included.

Deglycosylation scans were performed using constrained PCM-B3LYP/6-31G(d) optimizations in the solvent (water) phase. In these calculations, only the C−N bond length was constrained, where it was gradually increased in 0.1 Å increments and optimized at each step from 1.4 to 3.4 Å.

All B3LYP calculations were performed using Gaussian 03.[41]

Acknowledgment. Support for this research was provided by the Natural Sciences and Engineering Research Council

(40) Spartan ′02 Wavefunction, Inc. Irvine, CA.

(41) Frisch, M. J.; Trucks, G. W.; Schlegel, H. B.; Scuseria, G. E.; Robb, M. A.; Cheeseman, J. R.; Montgomery, J. A., Jr.; Vreven, T.; Kudin, K. N.; Burant, J. C.; Millam, J. M.; Iyengar, S. S.; Tomasi, J.; Barone, V.; Mennucci, B.; Cossi, M.; Scalmani, G.; Rega, N.; Petersson, G. A.; Nakatsuji, H.; Hada, M.; Ehara, M.; Toyota, K.; Fukuda, R.; Hasegawa, J.; Ishida, M.; Nakajima, T.; Honda, Y.; Kitao, O.; Nakai, H.; Klene, M.; Li, X.; Knox, J. E.; Hratchian, H. P.; Cross, J. B.; Bakken, V.; Adamo, C.; Jaramillo, J.; Gomperts, R.; Stratmann, R. E.; Yazyev, O.; Austin, A. J.; Cammi, R.; Pomelli, C.; Ochterski, J. W.; Ayala, P. Y.; Morokuma, K.; Voth, G. A.; Salvador, P.; Dannenberg, J. J.; Zakrzewski, V. G.; Dapprich, S.; Daniels, A. D.; Strain, M. C.; Farkas, O.; Malick, D. K.; Rabuck, A. D.; Raghavachari, K.; Foresman, J. B.; Ortiz, J. V.; Cui, Q.; Baboul, A. G.; Clifford, S.; Cioslowski, J.; Stefanov, B. B.; Liu, G.; Liashenko, A.; Piskorz, P.; Komaromi, I.; Martin, R. L.; Fox, D. J.; Keith, T.; Al-Laham, M. A.; Peng, C. Y.; Nanayakkara, A.; Challacombe, M.; Gill, P. M. W.; Johnson, B.; Chen, W.; Wong, M. W.; Gonzalez, C.; Pople, J. A. *Gaussian 03*, Revisions C.02 and D.01; Gaussian, Inc.: Wallingford, CT, 2004.

(NSERC) of Canada, the Canada Research Chair program, the Canada Foundation for Innovation, and the Ontario Innovation Trust Fund. R.A.M. thanks Ms. Karen Shipley for carrying out preliminary experiments. A.L.M. thanks NSERC and Alberta Ingenuity for student scholarships.

Supporting Information Available: General experimental procedures, ^{1}H and ^{13}C NMR spectra of adduct **3c**, and Cartesian coordinates for $N^{7}H^{+}$ of adducts **2b**, **3b**, and **2c**. This material is available free of charge via the Internet at http://pubs.acs.org.